RSC Advances Communication

Electronic Supplementary Information (ESI)

Large-Scale Nanopatterning of Metal Surfaces by Target-ion Induced Plasma Sputtering (TIPS)

Tae-Sik Jang [a], *Sungwon Kim* [a], *Hyun-Do Jung* [b], *Jin-Wook Chung* [c], *Hyoun-Ee Kim* [a], *Young-Hag Koh* [d], *and Juha Song* [a] *

**Corresponding to: Juha Song email: E-mail: sat105@snu.ac.kr*

A. Experimental methods

Plasma sputtering was conducted on metal alloy substrates using DC magnetron sputtering equipment (Ultech Co. Ltd., Korea) with a Ta target (75 mm diameter x 5 mm thickness, purity 99.99%, Kojundo, Japan). Prior to processing, commercially available metallic alloys (Co-Cr, NiTi, 316L stainless steel) were cleaned ultrasonically. The deposition chamber was pumped to 5 x 10^{-4} Pa using rotary and diffusion pumps. The substrate was then subjected to plasma etching in an argon (Ar) flow discharge under a negative bias voltage of 600 V for 15 min to remove any residual surface contamination. Subsequently, substrates were plasma etched up to 90 min at a target power of 60 W in a high-purity (99.998%) argon flow while negative substrate bias voltage was applied to the metal substrates. The substrate temperature was kept at 100 °C using a halogen heater with a programmable temperature controller.

The surface morphology and cross-sectional image of the nanopatterned alloy substrates were examined by atomic force microscopy (AFM, NanoStation II, Bruker, Germany) and field emission scanning electron microscopy (FE-SEM; SUPRA 55 VP, CARL ZEISS, Germany). The chemical composition of the Ta-treated metal substrates was characterized by energy dispersive spectroscopy (EDS) attached to the FE-SEM. For comparison purposes, the bare metal substrates were also tested. The cross-sectional morphologies of the nanostructured surface was fabricated and analyzed by FIB (AURIGA) and TEM (JEM-2100F). The diffraction pattern and EDS spot analysis were performed in order to identify the crystal structure and chemical composition in the nano-probe (beam diameter ~2nm) TEM mode.

B. DC Magnetron sputtering

DC magnetron sputtering equipment is one of the most widely used surface modification techniques that allows the fast deposition of various types of metals onto substrate by the use of applied DC power to the target. The negative bias applied to the substrate during deposition process can attract high energetic positive ions (Ar^+, target ions), and increase substrate surface temperature and mobility of adsorbed atoms, which leads to strong adhesive and texture deposited film layer on the substrat.[1] If the substrate bias voltage is even higher than the binding energy of substrate atoms, introduced energetic ion bombardment phenomenon of the surface provides excessive energy to the deposited film.[2]

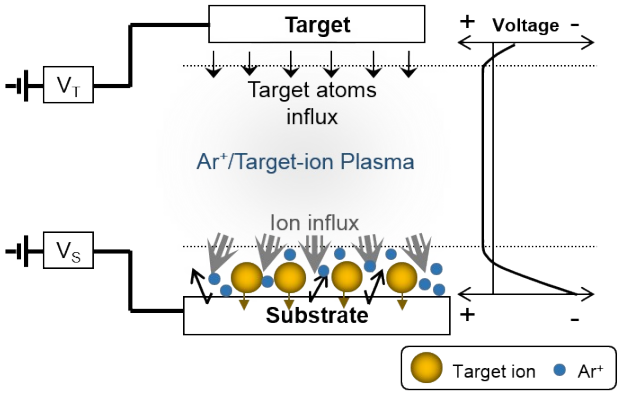

Figure S1. . Schematics of a DC magnetron sputtering process varying with substrate bias voltage (V_S) from 0V to -1600V. V_T is the target voltage, -200 V for this study.

C. EDS analysis of ripples on the Co-Cr substrate

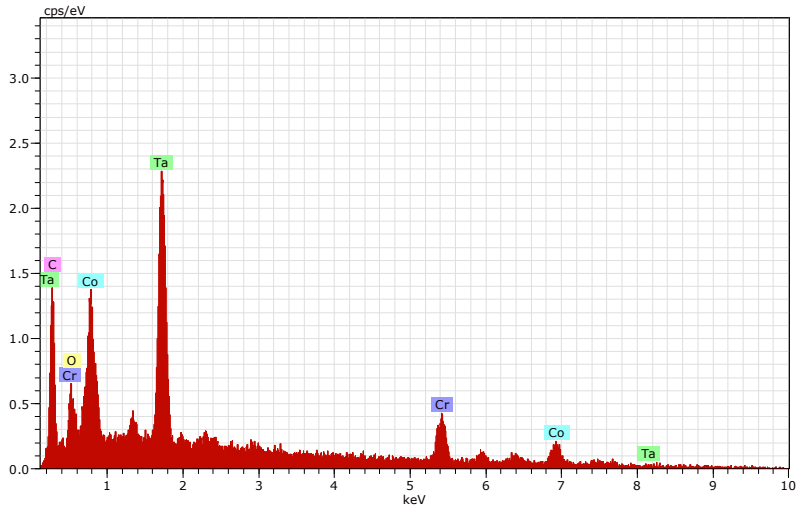

Figure S2. EDX spectrum of Ta-incorporated Co-Cr surface layer on the Co-Cr substrate

D. **Cross sectional Composition analysis of nanopatterned Co-Cr surface**

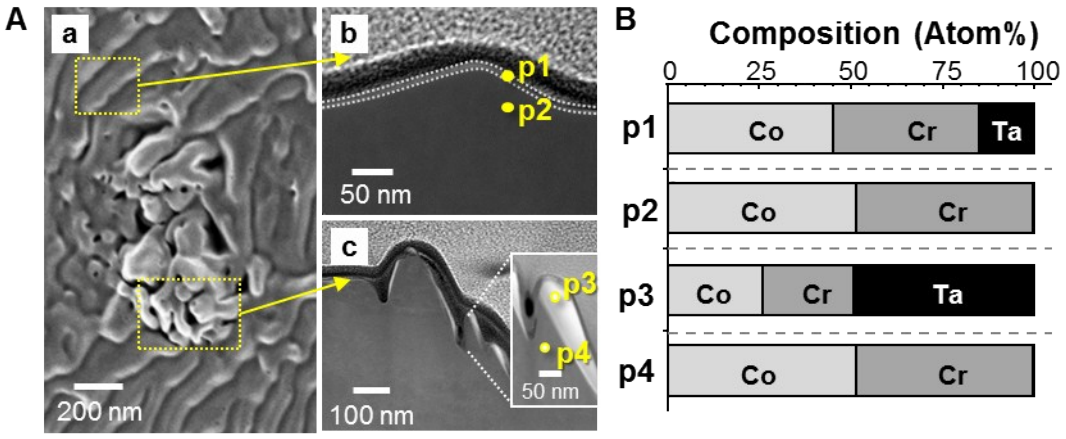

Figure S3. A) Top-view SEM image of nanopatterned Co-Cr (a) after 5 min of plasma sputtering, and its corresponding cross-sectional TEM images of ripples (b) and cluster (c). B) Chemical composition graphs of four spots (p1 to p4) indicated in (b) and (c).

E. **Optical property of ripple-patterned metal surfaces**

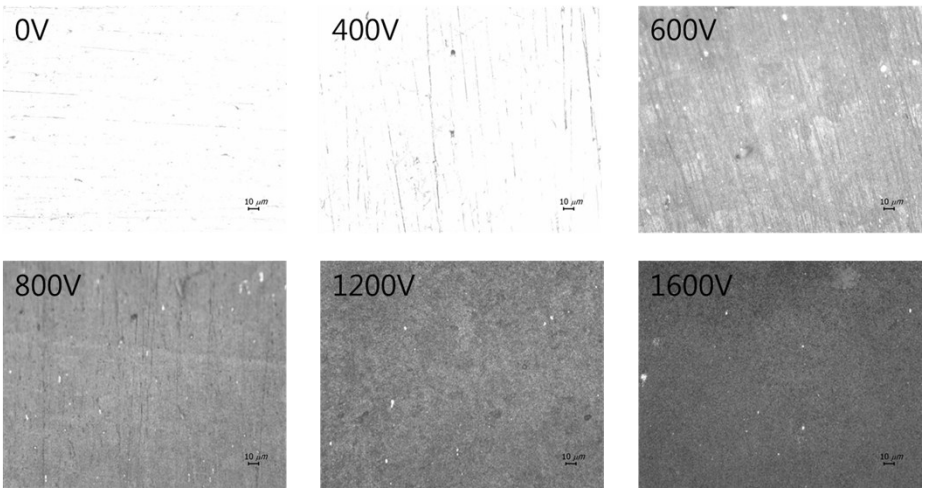

Figure S4. Optical images of ripple-patterned Co-Cr surfaces modified by TIPS, varying the substrate bias voltage

F. Formation of nanopatterns on NiTi and SUS over time

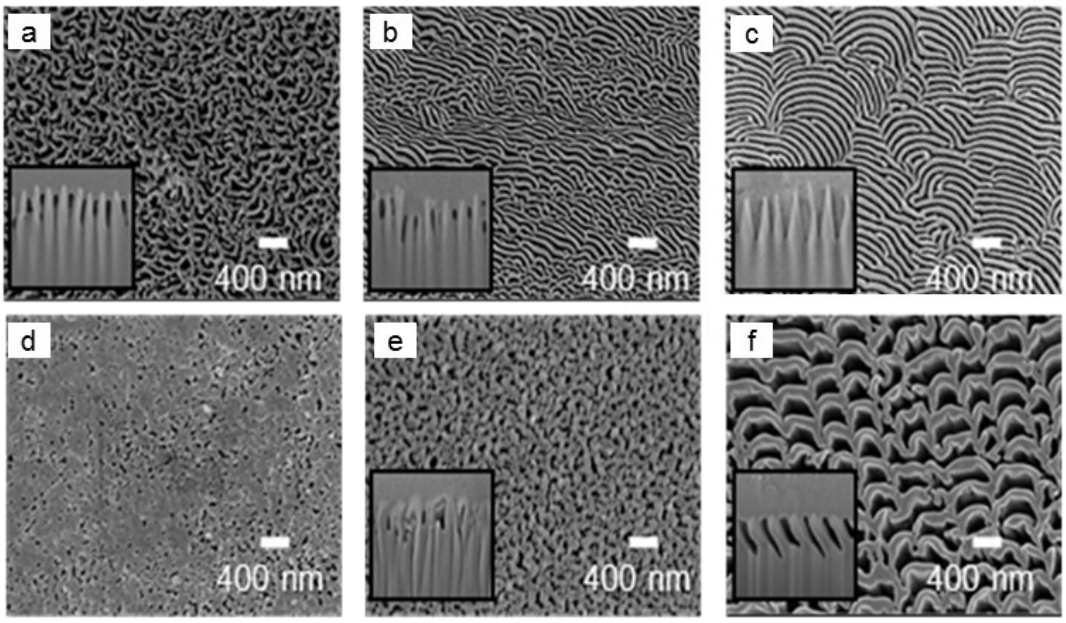

Figure S5. Top-surface and cross-sectional SEM images of NiTi obtained after different process times (a;10min, b; 30min, and c; 60min) and SUS obtained after different process times (d;10min, e; 30min, and f; 60min).

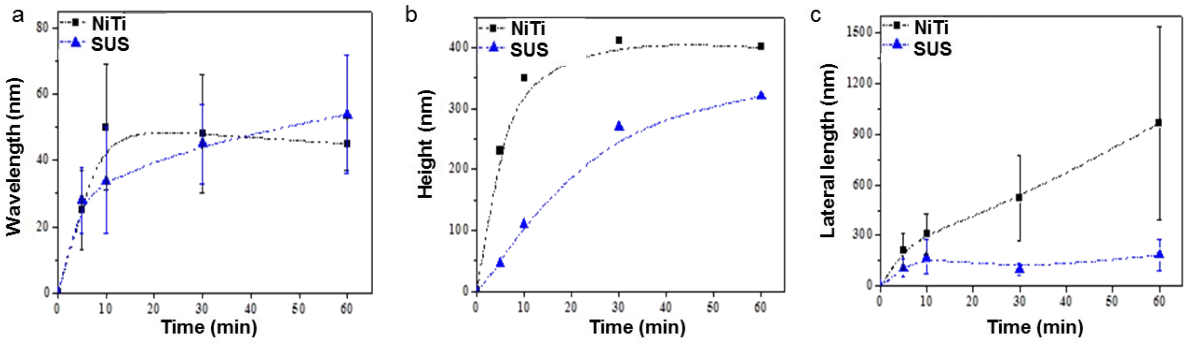

Figure S6. Topography evolution graphs of average wavelength (a), average height (h), and average lateral length of ripples on NiTi and SUS substrates over processing time

G. **Formation of naopatterns on a Co-Cr tube with complex geometry**

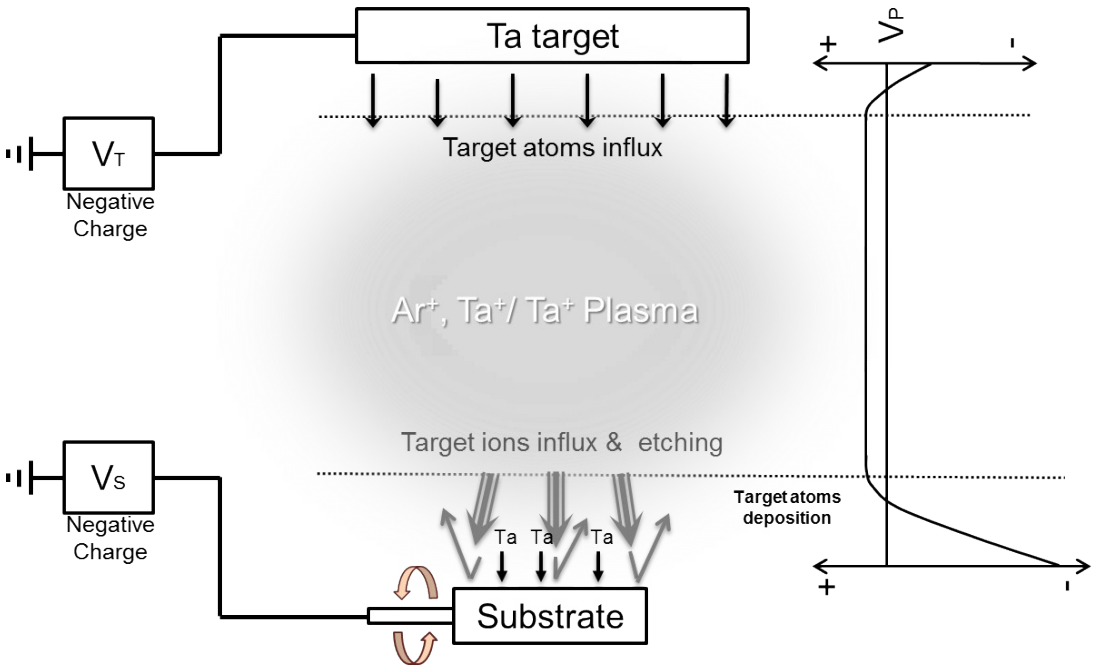

Figure S7. Schematics of a DC magnetron sputtering process with a rotating substrate with substrate bias voltage of -800V

A. Normalized surface area and pore volume of ripples on metal surfaces

The dimensions of ripple patterns were mainly controlled by time and substrate bias voltage. The normalized surface area (actual surface area/projected surface area) and pore volume of ripple-patterned surfaces were predicted, varying the pattern width (λ) with the fixed aspect ratio of the pattern depth and width as ~2.5, approximated from Fig. 3B (Fig. S8 and Fig. S9† in ESI). Regardless of the increased pattern depth, the surface area of ripples appeared > 5.5 times larger than their projected surface area. Moreover, the pore volume of a ripple pattern was increased linearly along with the increment of the pattern width. The large surface area and pore volume capacity of ripple structures on metal surfaces through TIPS could be used as "carriers" for trapping biomolecules, drugs, organic dyes or nanoparticles for the development of functional biomedical devices, biosensors, optoelectronics and magnetic media for high-density storage.[3, 4] Moreover, the unique surface topography of ripple patterns on metals could facilitate the alignment of biomolecules (e.g., DNA) or metal oxide nanowires (Fe_2O_3).[5-7]

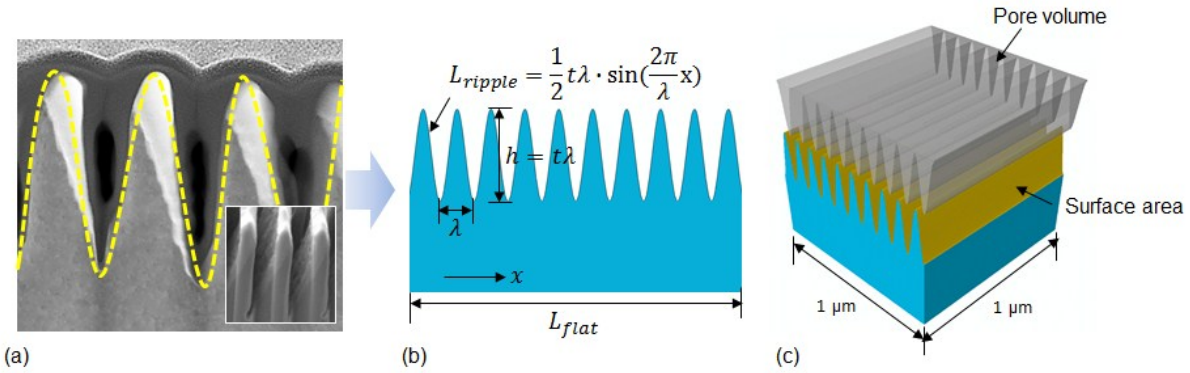

Figure S8. Schematic diagram of a ripple-patterned surface: (a) Image analysis of a ripple structure created on a metal surface, (b) 2D representative cross-section area of a ripple with curve fitting with a sine curve and (c) 3D unit cell of a ripple patterned metal system with corresponding surface area and pore volume of the ripple structure.

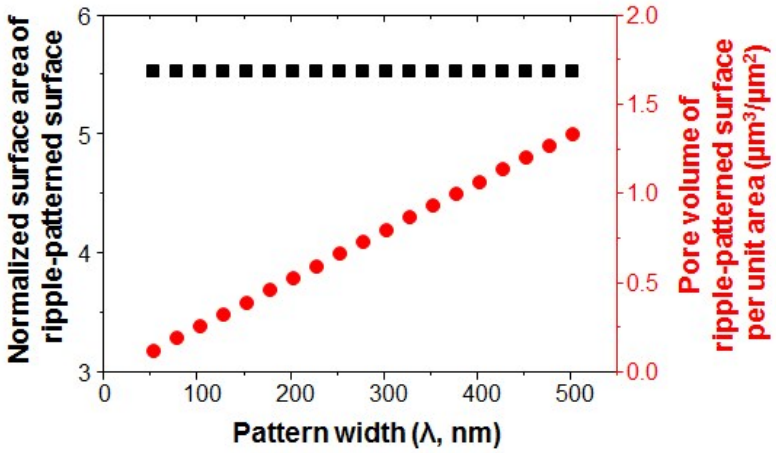

Figure. S9. Predicted values of normalized surface area (*actual surface area/projected surface area)* and pore volume of a ripple structure as a function of pattern width, assuming the ratio of pattern width and depth (t) is 2.5

References

1. P. J. Kelly and R. D. Arnell, *Vacuum*, 2000, **56**, 159-172.
2. V.-H. Pham, T.-S. Jang, H.-D. Jung, H.-E. Kim and Y.-H. Koh, *Journal of Materials Chemistry*, 2012, **22**, 24798.
3. T. Kumeria, A. Santos, M. M. Rahman, J. Ferre-Borrull, L. F. Marsal and D. Losic, *Acs Photonics*, 2014, **1**, 1298-1306.
4. K. F. Huo, B. Gao, J. J. Fu, L. Z. Zhao and P. K. Chu, *Rsc Adv*, 2014, **4**, 17300-17324.
5. Q. He, T. Yuan, Y. Wang, A. Guleria, S. Wei, G. Zhang, L. Sun, J. Liu, J. Yu, D. P. Young, H. Lin, A. Khasanov and Z. Guo, *Nanoscale*, 2016, **8**, 1915-1920.
6. Q. L. He, T. T. Yuan, X. R. Yan, Z. P. Luo, N. Haldolaarachchige, D. P. Young, S. Y. Wei and Z. H. Guo, *Chem Commun*, 2014, **50**, 201-203.
7. B. Teshome, S. Facsko and A. Keller, *Nanoscale*, 2014, **6**, 1790-1796.